Published in final edited form as:
Dev Biol. 2004 December 15; 276(2): 403–415. doi:10.1016/j.ydbio.2004.09.002.

Role of fibroblast growth factor receptors 1 and 2 in the ureteric bud

Haotian Zhao[a], **Heather Kegg**[a], **Sandy Grady**[a], **Hoang-Trang Truong**[b], **Michael L. Robinson**[a], **Michel Baum**[b], and **Carlton M. Bates**[a,c,*]

[a]Center for Human and Molecular Genetics, Columbus Children's Research Institute, Columbus, OH 43205, United States

[b]Department of Pediatrics, Division of Nephrology, University of Texas Southwestern Medical Center at Dallas, Dallas, TX 75235, United States

[c]Department of Pediatrics, Division of Nephrology, College of Medicine and Public Health, The Ohio State University, Columbus, OH 43210, United States

Abstract

Fibroblast growth receptors (FGFRs) consist of four signaling family members. Mice with deletions of *fgfr1* or *fgfr2* are embryonic lethal prior to the onset of kidney development. To determine roles of FGFR1 and FGFR2 in the ureteric bud, we used a conditional targeting approach. First, we generated transgenic mice using the Hoxb7 promoter to drive cre recombinase and green fluorescent protein expression throughout ureteric bud tissue. We crossed Hoxb7creEGFP mice with mice carrying lox-p sites flanking critical regions of *fgfr1* and/or *fgfr2*. Absence of *fgfr1* from the ureteric bud ($fgfr1^{UB-/-}$) results in no apparent renal abnormalities. In contrast, $fgfr2^{UB-/-}$ mice have very aberrant ureteric bud branching, thin ureteric bud stalks, and fewer ureteric bud tips. $Fgfr2^{UB-/-}$ ureteric bud tips also demonstrate inappropriate regions of apoptosis and reduced proliferation. The nephrogenic mesenchymal lineage in $fgfr2^{UB-/-}$ mice develops normal-appearing glomeruli and tubules, and only slightly fewer nephrons than controls. In contrast, $fgfr2^{UB-/-}$ kidneys have abnormally thickened subcapsular cortical stromal mesenchyme. Ultimately, $fgfr2^{UB-/-}$ adult kidneys are small and abnormally shaped or are hydronephrotic. Finally, there are no additional abnormalities in the $fgfr1/2^{UB-/-}$ kidneys versus the $fgfr2^{UB-/-}$ kidneys. In conclusion, FGFR2, but not FGFR1, appears crucial for ureteric bud branching morphogenesis and stromal mesenchyme patterning.

Keywords

Fibroblast growth factor receptors; Kidney development; Ureteric bud; Branching morphogenesis; Stromal patterning; Conditional knockout

*Corresponding author. Center for Human and Molecular Genetics, Columbus Children's Research Institute, 700 Children's Drive Columbus, Ohio 43205. Fax: +1 614 722 2817. batesc@pediatrics.ohio-state.edu (C.M. Bates).

Introduction

Fibroblast growth factor receptors (FGFRs) are a gene family of receptor tyrosine kinases with at least 4 signaling members (Powers et al., 2000). Three of these genes (*fgfrs1-3*) are capable of producing multiple receptor isoforms through alternative splicing of primary transcripts (Powersetal., 2000). Fibroblast growth factor receptors are activated by binding to FGF ligands, of which there are 22 known family members in mammals (Powers et al., 2000). Structurally, the receptors consist of up to three external immunoglobulin-like domains, a transmembrane (TM) domain, and an intracellular kinase domain (Powers et al., 2000). Alternate splicing of the C-terminal portion of the third Ig-like domain results in IIIb or IIIc isoforms, which have different ligand binding specificities (Powers et al., 2000). In vitro, FGFR activation is associated with many biological responses including proliferation, differentiation, migration, and inhibition of apoptosis (Klint and Claesson-Welsh, 1999). Finally, fibroblast growth factor receptors are expressed in many tissues of the developing embryo starting prior to implantation and often persisting into adulthood.

The metanephric kidney develops from 2 tissues arising from the intermediate mesoderm, the Wolffian duct and the nephrogenic cord (Kuure et al., 2000). Between gestational ages 10.5–11.0 in the mouse, the nephrogenic cord gives rise to the metanephric mesenchyme that then induces the formation of the ureteric bud from the Wolffian duct in the region of the hindlimb (Kuure et al., 2000). Shortly afterward, the metanephric mesenchyme divides into a nephrogenic lineage lying adjacent to the ureteric bud, and a stromal lineage that surrounds the nephrogenic mesenchyme (Kuure et al., 2000). The tissues then begin a series of reciprocal inductive interactions, with the ureteric bud receiving signals to branch dichotomously, ultimately to form the collecting ducts and ureter (Kuure et al., 2000). At each terminal tip, the ureteric bud induces local areas of nephrogenic mesenchyme to differentiate into nephron epithelia (Kuure et al., 2000). In addition to interactions between the nephrogenic and ureteric bud lineage, others have recently documented critical signaling between ureteric bud and stromal lineages (Batourina et al., 2001; de Graaff et al., 2001; Mendelsohn et al., 1999).

Although several studies have reported finding *fgfrs* in the developing mammalian kidney, the data on specific expression patterns in the embryonic kidney are ambiguous (Cancilla et al., 1999; Dudley et al., 1999; Fuhrmann et al., 1999; Peters et al., 1992). One study in mice reported that *fgfr1* was present only in nephrogenic mesenchyme-derived tissues by in situ hybridization (Peters et al., 1992). Another report in rats, however, described *fgfr1* expression in all ureteric bud and nephrogenic mesenchymal lineages by in situ hybridization and immunohistochemistry (Cancilla et al., 1999). The studies on *fgfr2* in rodents have all reported expression in the ureteric bud, although there are disagreements over the level and timing of expression in mesenchymal derivatives (Cancilla et al., 1999; Dudley et al., 1999; Peters et al., 1992).

The importance of FGFR signaling in the developing kidney was first demonstrated when transgenic mice with a dominant negative FGFR fragment were found to possess no kidneys or very small dysplastic kidney rudiments (Celli et al., 1998). Despite this, gene targeting approaches have only revealed limited data on which *fgfrs* are important in the developing

kidney. Mice with targeted deletions of *fgfr1* die during or shortly gastrulation, prior to the onset of renal development (Deng et al., 1994; Yamaguchi et al., 1994). Although two groups reported different phenotypes in their respective *fgfr2* null mice, both strains were also embryonic lethal before the kidney starts to form (Arman et al., 1998; Xu et al., 1998). Mice with targeted deletions of *fgfr3* and *fgfr4* are viable and do not have kidney abnormalities (Colvin et al., 1996; Weinstein et al., 1998). Mice null for *fgf7*, *fgf10*, and *fgfr2-IIIb* (the main receptor isoform for FGF7 and FGF10), do have slightly small kidneys, but all have normal-appearing nephrons (Ohuchi et al., 2000; Qiao et al., 1999; Revest et al., 2001).

Our objective was to determine the roles of FGFR1 and FGFR2 in the ureteric bud, using a conditional targeting approach. First, we generated transgenic mice using the Hoxb7 promoter to drive expression of cre recombinase and green fluorescent protein throughout ureteric bud tissue. Then, we crossed Hoxb7creEGFP mice with mice carrying lox-p sites flanking critical regions of *fgfr1* and/or *fgfr2*. Absence of *fgfr1* from the ureteric bud results in no apparent renal abnormalities. In contrast, $fgfr2^{UB-/-}$ mice have thin ureteric bud stalks, fewer total ureteric tips, and fewer tips per surface area. $Fgfr2^{UB-/-}$ ureteric tips also demonstrate inappropriate regions of apoptosis and reduced proliferation. The nephrogenic mesenchymal lineage in the $fgfr2^{UB-/-}$ mice develops normal-appearing glomeruli and tubules, and only slightly fewer nephrons than controls. In contrast, the $fgfr2^{UB-/-}$ kidneys have abnormally thickened cortical stromal mesenchyme with excessive apoptosis. Ultimately, $fgfr2^{UB-/-}$ adult kidneys are small and abnormally shaped or are hydronephrotic.

Materials and methods

Generation of Hoxb7creEGFP mice and the conditional knockout mice

We received a vector containing a portion of the Hoxb7 promoter (extending from −1316 to 181 of the genomic fragment) followed by a 1.7-kb fragment of the human β globin gene containing the polyadenylation (poly-A) signal sequence (gift from Dr. Frank Costantini, Columbia University, New York). The Hoxb7 promoter fragment has been used by others to misexpress genes such as an enhanced green fluorescent protein (EGFP) (Srinivas et al., 1999a), *Ret* (Srinivas et al., 1999b), and cre recombinase (Yu et al., 2002). We then cloned in a cre recombinase open reading frame (ORF) immediately downstream of the promoter fragment followed by an internal ribosomal entry site (IRES) and enhanced green fluorescent protein (EGFP) ORF (derived from the pIRES2-EGFP vector from Clontech/BD Biosciences) (see Fig. 1). After linearizing, we injected the construct into mouse zygote pronuclei. We identified three founder mice by polymerase chain reaction (PCR) (see Table 1) followed by Southern blotting using the fragment amplified from the PCR primers. We bred the founder mice with FVB/N mice and confirmed genotypes in the F1 offspring as above.

To characterize the expression of the three lines, we first examined whole kidneys dissected at embryonic day (E) 14.5 under fluorescent light for the presence of GFP. We did the same with explants dissected at E11.5 and grown for 3 days in Dulbecco's modified Eagle medium (DMEM) (GIBCO) with 10% fetal bovine serum (FBS) (GIBCO). To test for cre recombinase activity, we bred the Hoxb7-creEGFP lines with cre-responsive β-galactosidase

reporter mice (G*trosa*26^{tm1Sor}) (Soriano, 1999). After fixing whole E11.5 embryos overnight and E14.5 kidneys for 6 h with 4% paraformaldehyde (PFA) in phosphate-buffered saline (PBS), we X-gal stained the tissues overnight at room temperature with 5 mM potassium ferricyanide, 5 mM potassium ferrocyanide, 4-chloro-5-bromo-3-indolyl-*b*-D-galactopyranoside, 0.1% deoxycholate, 0.2% Nonidet P-40, 2 mM $MgCl_2$ in PBS. Two of the lines (5526 and 5530) had specific expression in the ureteric bud epithelia and we used the line with the strongest expression (5526) for all subsequent studies.

To generate the conditional *fgfr* knockouts, we first obtained mice with lox-p sites flanking critical regions (floxed) of *fgfr1* (gift from Dr. Janet Rossant, Samuel Lunenfeld Research Institute, Toronto, Canada (Hebert et al., 2003) and *fgfr2* (gift from Dr. David Ornitz, Washington University, St. Louis (Yu et al., 2003). Genotyping for the *fgfr1* and *fgfr2* alleles were by PCR (see Table 1). We then bred the hemizygous Hoxb7creEGFP mice (cre$^{+/-}$) with mice that were compound homozygous for the floxed *fgfr1* and *fgfr2* alleles (*fgfr1*$^{lox/lox}$, *fgfr2*$^{lox/lox}$). We then bred cre-positive progeny (cre$^{+/-}$, *fgfr1*$^{lox/+}$, *fgfr2*$^{lox/+}$) back with the compound homozygous parental mice (*fgfr1*$^{lox/lox}$, *fgfr2*$^{lox/lox}$). Subsequent Hoxb7creEGFP-positive progeny contained mice with deletion of *fgfr1*, *fgfr2*, or both *fgfr1/2*, or that were compound heterozygotes (see Table 2).

Explant and whole kidney studies

We removed embryonic kidney rudiments at E11.5 and cultured them on nucleopore filters floating on DMEM with 10% FBS at 37°C for 3 days. We then photographed the GFP-positive ureteric bud trees in littermate double heterozygous, *fgfr1*$^{UB-/-}$, *fgfr2*$^{UB-/-}$, and *fgfr1/2*$^{UB-/-}$ explants and tabulated the mean number of ureteric bud tips for each group. To visualize the developing glomeruli, we also performed whole mount immunofluorescence on methanol-fixed littermate explants with a polyclonal antibody against Wt1 (Santa Cruz) in the manner we described previously (Bates et al., 2000). We tabulated the mean number of glomeruli in the double heterozygous, *fgfr1*$^{UB-/-}$, *fgfr2*$^{UB-/-}$, and *fgfr1/2*$^{UB-/-}$ explants. We compared the mean number of ureteric bud tips and glomeruli for 4 cre-positive groups with a one-way analysis of variance (ANOVA) ($P < 0.05$ was considered significant). We also compared mean numbers glomeruli in littermate double heterozygous and cre-negative explants by unpaired T tests ($P < 0.05$ was considered significant).

We removed and photographed kidneys from E13.5, E16.5, and 6-week-old mice under direct light and tabulated mean lengths of E16.5 littermate double heterozygous, *fgfr1*$^{UB-/-}$, *fgfr2*$^{UB-/-}$, *fgfr1/2*$^{UB-/-}$, and cre-negative kidneys. We also photographed the embryonic kidneys from the first four (cre-positive) groups under fluorescent light to visualize the GFP-positive ureteric bud trees. We also performed confocal microscopy on the cre-positive E16.5 kidneys, capturing a total of thirty 10-μm-thick sections/per kidney that were then compressed into a single image. We compared the mean length, number of ureteric bud tips and number of ureteric tips/surface area of each of the 4 cre-positive groups a one-way analysis of variance (ANOVA) ($P < 0.05$ was considered significant). We also compared mean lengths of double heterozygous and cre-negative explants by unpaired *t* tests ($P < 0.05$ was considered significant).

Histological experiments on tissue sections

We performed hematoxylin and eosin (H&E) staining on PFA-fixed, paraffin embedded E13.5, E16.5, and adult kidney tissues from littermate double heterozygous, *fgfr1*$^{UB-/-}$, *fgfr2*$^{UB-/-}$, *fgfr1/2*$^{UB-/-}$, and cre-negative mice (reagents from Richard-Allen Scientific). We also performed immunofluorescence on Histochoice (Amresco)-fixed, cryostat-sectioned E13.5 and E16.5 littermate kidney sections with primary rabbit polyclonal antibodies against FGFR1 (Santa Cruz, catalog #sc-121), FGFR2 (Santa Cruz, catalog #sc-122), Wt1 (Santa Cruz, catalog #sc-192) and GFP (Molecular Probes, catalog #A-11122) at 1:100, 1:100, 1:20, and 1 μg/mL, respectively. We used secondary antibodies including goat anti-rabbit Cyanine (Cy) 2 conjugates (for the GFP antibody) (Jackson Immunochemicals) and anti-rabbit Cy3 conjugates (for the other primary antibodies) (Jackson Immunochemicals) at 1:250, and 1: 500, respectively. We performed immunofluorescence as we described previously (Bates et al., 2003).

We performed radioactive in situ hybridization in PFA-fixed, paraffin embedded E13.5 and E16.5 littermate kidney sections using cDNA templates against *fgfr1* (nucleotides 1546–1996 of GenBank accession no. NM010206) and *fgfr2* (nucleotides 1594–1941 of GenBank accession no. X55441). The cDNA templates contain sequence of exons that should be deleted in the conditional knockout mice (Hebert et al., 2003; Yu et al., 2003). We generated ^{35}S-UTP-labeled antisense RNA probes against the cDNA templates and performed in situ hybridization with the probes as we described previously (Bates et al., 1997).

We performed non-radioactive in situ hybridization in E13.5 littermate kidney sections using cDNA templates against *Foxd1* (nucleotides 1693–2690 of GenBank accession no. L38607) (gift from Dr. Larry Patterson, University of Cincinnati, Cincinnati, Ohio) and *Ret* (nucleotides 3205–3688 of GenBank accession no. BC059012). We generated digoxigenin-UTP-labeled antisense RNA probes using the DIG RNA labeling kit (Roche). After deparaffinizing the sections, we hydrated, fixed with 4% PFA for 30 min, treated with 0.2 N HCl for 5 min, and then digested with 20 μg/mL of proteinase K (Invitrogen) at 37°C for 10 min. We then post fixed in 4% PFA for 10 min, treated with 0.1 M triethanolamine freshly supplemented with 625/250 mL of acetic anhydride for 10 min with stirring, and dehydrated the sections. After the slides dried, we added denatured probe diluted to 2 μg/mL in hybridization buffer (Sigma) with 100 μg/mL tRNA to slides, applied coverslips, and incubated overnight at 55°C in humidifying chambers. We washed the tissues with 5× SSC and then 2× SSC in 10 mM DTT at 50°C for 30 min each. We then incubated sections for 30 min with 20 μg/mL RNAse A and 100 U/mL of RNAse T1 at 37°C. We then blocked for 30 min in a solution of MAB (100 mM maleic acid, 150 mM NaCl pH 7.5) containing 0.1% Tween and 2 mM levamisole. We then incubated with an anti-DIG antibody (Roche) diluted 1:2000 in MAB over night at 4°C. After three 10-min washes of MAB with 0.1% Tween, we washed the sections twice for 5 min with AP development buffer (10 mM Tris–Cl pH 9.5, 2 mM levamisole, 500 mM NaCl, 0.1% Tween-20, 5 mM $MgCl_2$). We then placed the slides in a humidity chamber and incubated them in BM purple AP substrate solution (Roche) for 1 week. After stopping the reaction with three 5-min PBS washes, we

dehydrated, clarified, and added coverslips with aqueous mounting media. For the *Foxd1* samples, we also counterstained with nuclear fast red prior to dehydrating the sections.

We performed apoptosis and proliferation assays in double heterozygous and *fgfr2*$^{UB-/-}$ littermate embryonic kidney sections. To detect apoptosis in E13.5 and E16.5 PFA-fixed, paraffin-embedded sections, we used the Fluorescent FragEl DNA Fragmentation Detection kit (Oncogene). Briefly, we deparaffinized, hydrated, and permeabilized the tissues with proteinase K. We then incubated the sections with terminal transferase (TdT) equilibration buffer for 30 min followed by the labeling reaction mixture with TDT enzyme for 1 h at 37°C. We then washed the slides and added coverslips with aqueous mounting media. To measure cell proliferation, we performed bromodeoxyuridine (BrdU) assays on Histochoice-fixed, paraffin-embedded E13.5 kidney sections, as exactly described previously (Bates et al., 2000). To quantitate ureteric bud proliferation rates in the cortex, we serially sectioned 6 *fgfr2*$^{UB-/-}$ and 6 control littermates (6 μm sections). On average, we stained every 10th *fgfr2*$^{UB-/-}$ section and every 12th control section for BrdU as above (5 sections total). We then counted numbers of BrdU-positive (brown) and -negative (blue) cells in the ureteric bud tissues throughout the cortex in one kidney per embryo. On average, we counted 531 *fgfr2*$^{UB-/-}$ ureteric bud cells and 865 control ureteric bud cells. We calculated proliferation rates in ureteric bud tips from the ratio of BrdU-positive to total nuclei. We then compared percentages of proliferation with unpaired t tests with a $P < 0.05$ considered significant (as described previously) (Bates et al., 2000).

Adult kidney glomerular counts

We determined glomerular number in double heterozygous and *fgfr2*$^{UB-/-}$ 6-week-old littermate mouse kidneys using a variation of the technique of Damadian et al. (1965) with significant modifications (Bankir and Hollenberg, 1983; Gilbert et al., 1987) as we recently described (Ortiz et al., 2001, 2003). We anesthetized the mice with 0.1–0.15 mg/g body weight of Inactin and then opened the chest to expose the heart. We infused 2 mL of a 1.25% solution of Alcian blue (Aldrich Chemical Company) in normal saline over 1 min into the left ventricle to stain glomeruli (Bankir and Hollenberg, 1983; Gilbert et al., 1987; Ortiz et al., 2001, 2003). After removing the kidneys, we sliced them in half, and incubated in 5 cc of 27% ammonium hydroxide for 2 h at room temperature. We then treated the kidneys with 5 mL of 8 N HCl at 50°C for 1 h. We diluted the suspension to a final volume of 20 mL with water and incubated overnight at 4°C. We counted the number of glomeruli in ten 30 μL samples using a light microscope and tabulated the mean number of glomeruli per kidney. We then compared mean glomerular numbers with unpaired *t* tests ($P < 0.05$ was considered significant).

Microscopy and photography

We captured all images on a MagnaFire digital camera (Optronics) mounted on a Leica DM LB microscope and then converted them to Adobe Photoshop files. We used a Zeiss LSM 410 microscope for the confocal studies.

Results

Characterizing Hoxb7creEGFP mice and generation of fgfr1 and fgfr2 conditional knockouts in the ureteric bud

To characterize the Hoxb7creEGFP mice, we first examined embryonic tissues directly for GFP expression. We detected specific GFP signal in the ureteric bud epithelia in E11.5 explants (Fig. 2b) and in E14.5 whole kidneys (Fig. 2d). To confirm that the cre recombinase was active and to evaluate transgene expression elsewhere in the embryo, we then bred the transgenic mice with cre-responsive β-galactosidase reporter mice. After X-gal staining, we detected β-galactosidase in E11.5 embryonic ureteric buds (Figs. 2f, g, arrows) and Wolffian ducts (Fig. 2g, concave arrow) and in isolated embryonic kidney ureteric bud epithelia (Fig. 2i). We also detected transgene expression in the hindbrain regions of the embryos (Fig. 2f, arrowhead), as is the case in other transgenic mice with the Hoxb7 promoter (Dr. Frank Costantini and Dr. Andrew McMahon, personal communications). We then crossed the Hoxb7-creEGFP mice with floxed *fgfr1* and/or *fgfr2* mice, according the breeding scheme outlined in Materials and methods and Table 2. In overall appearance as well as in assays including histological staining, kidney length, and explant ureteric bud and glomerular counts, double heterozygous mice were indistinguishable from cre-negative mice; therefore, unless otherwise indicated, we used double heterozygotes as controls in comparison with $fgfr1^{UB-/-}$, $fgfr2^{UB-/-}$, and $fgfr1/2^{UB-/-}$ mice.

To determine efficiency of *fgfr* deletion from the ureteric bud in the conditional knockouts, we first determined whether we could detect *fgfr* expression in control ureteric bud tissues in by immunostaining and/or in situ hybridization; if so, we would then compare *fgfr* expression in control and $fgfr^{UB-/-}$ mouse kidneys. By in situ hybridization and immunofluorescence for *fgfr1* at E13.5 and E16.5, we detected signal in regions of control double heterozygous kidneys including tubules that did not appear to be ureteric bud tissues (Fig. 3b and not shown). Immunostaining in serial sections of E16.5 control kidneys confirmed that FGFR1-expressing tubules (Fig. 3b, arrowhead) were not GFP-positive ureteric bud epithelia (Fig. 3a, arrows). In contrast, while *fgfr2* expression by in situ hybridization appeared in some control mesenchyme tissues, especially those immediately adjacent to the ureteric bud (Figs. 3c and d, concave arrowheads), the most intense signal was in the ureteric bud epithelia (Figs. 3c and d, concave arrows). In $fgfr2^{UB-/-}$ conditional knockout mice, the mesenchyme continued to express *fgfr2* by in situ hybridization (Figs. 3e and f, concave arrowheads); however, the ureteric bud signal was completely absent (Figs. 3e and f, concave arrowheads). Thus, we confirmed that the $fgfr2^{UB-/-}$ conditional knockout had very efficient deletion of *fgfr2* in the ureteric bud epithelia.

$Fgfr2^{UB-/-}$ embryonic kidneys are small and adult kidneys are abnormally shaped or hydronephrotic, while $fgfr1^{UB-/-}$ are normal

We dissected and examined embryonic and adult kidneys for phenotypic abnormalities. At E13.5 (not shown) and E16.5, $fgfr2^{UB-/-}$ kidneys (Fig. 4c) and $fgfr1/2^{UB-/-}$ kidneys (not shown) were smaller than control (Fig. 4a) and $fgfr1^{UB-/-}$ kidneys (Fig. 4b), although a fluorescent GFP-positive ureteric bud tree was apparent in all genotypes (Figs. 4d–f). Measurements of kidney lengths at E16.5 confirmed that mean sizes of both $fgfr2^{UB-/-}$ (1.47

mm ± 0.8, $N = 12$) and the *fgfr1/2*$^{UB-/-}$(1.40 mm ± 0.06, $N = 14$) were smaller than control (2.09 mm ± 0.07, $N = 18$) ($P < 0.0001$) and *fgfr1*$^{UB-/-}$ kidneys (2.07 mm ±0.7, $N = 8$) ($P < 0.0001$). There were no statistical differences in mean lengths of *fgfr2*$^{UB-/-}$ and *fgfr1/2*$^{UB-/-}$ kidneys or of control and *fgfr1*$^{UB-/-}$ kidneys. Although mice of all genotypes are viable after birth, approximately 80% of the *fgfr2*$^{UB-/-}$ adult mice have small, abnormally shaped kidneys (Fig. 4h) and the other 20% have hydronephrosis (Fig. 4i) which occurs unilaterally or bilaterally. Similar renal phenotypes are present in *fgfr1/2*$^{UB-/-}$ mice (not shown) and *fgfr1*$^{UB-/-}$ kidneys are indistinguishable from controls (not shown). Despite the abnormalities in their kidneys, *fgfr2*$^{UB-/-}$ and *fgfr1/2*$^{UB-/-}$ live born mice do not have any obvious external abnormalities and are the same sizes as control and *fgfr1*$^{UB-/-}$ mice through adulthood (not shown). In addition, among the 36 hoxb7cre– positive adult mice (from the crosses outlined in Table 2), 17 are either double heterozygotes or *fgfr1*$^{UB-/-}$ and the other 19 are either *fgfr2*$^{UB-/-}$ or *fgfr1/2*$^{UB-/-}$. The exact numbers of mice for each genotype are listed in Table 3.

Fgfr2$^{UB-/-}$ mice have profound abnormalities in ureteric bud development, while fgfr1$^{UB-/-}$ mice are normal

To characterize any defects in the ureteric bud lineage in the *fgfr1*$^{UB-/-}$ and/or *fgfr2*$^{UB-/-}$ mice, we examined GFP-positive ureteric bud tissues in E11.5 explants and E16.5 kidneys. *Fgfr1*$^{UB-/-}$ explants (Fig. 5b) were indistinguishable from controls (Fig. 5a). In contrast, *fgfr2*$^{UB-/-}$ explants had abnormally thin, long ureteric stalks and fewer peripheral tips, with a range in phenotype severity (compare Figs. 5c and d). *Fgfr1/2*$^{UB-/-}$ explants appeared similar to the *fgfr2*$^{UB-/-}$ mutants (not shown). Quantitatively, mean ureteric bud tip numbers between control (42.3 ± 2.0) and *fgfr1*$^{UB-/-}$ (44.1 ± 2.5) were statistically no different, as was true between *fgfr2*$^{UB-/-}$ (24.6 ± 3.1) and *fgfr1/2*$^{UB-/-}$ (22.8 ± 2.3). However, both control and *fgfr1*$^{UB-/-}$ explants had statistically higher mean ureteric bud tip numbers than both *fgfr2*$^{UB-/-}$ ($P < 0.0001$) and the *fgfr1/2*$^{UB-/-}$ explants ($P < 0.0001$) (Fig. 5e). Confocal analysis of isolated E16.5 kidneys revealed very similar data with dramatic decreases in mean ureteric bud tip numbers on the surface of *fgfr2*$^{UB-/-}$ (89.5 ± 14.1) and *fgfr1/2*$^{UB-/-}$ kidneys (98.2 ± 13.4) compared with either control (271 ± 15.4) ($P < 0.0001$) or *fgfr1*$^{UB-/-}$ kidneys (260 ± 24.2) ($P < 0.0001$) (Fig. 5f). Further analysis of E16.5 *fgfr2*$^{UB-/-}$ (and *fgfr1/2*$^{UB-/-}$) kidneys revealed a range in ureteric bud defects, including extremely small kidneys with large areas devoid of ureteric tissues (Fig. 6b, arrowheads). Even in mutants with less severe phenotypes, there appear to be fewer ureteric bud tips per surface area of the kidney (Fig. 4f). Confocal analysis of GFP-positive E16.5 kidneys confirmed that mean ureteric bud tip numbers/surface area (mm^2) in *fgfr2*$^{UB-/-}$ (19.5 ± 1.8) and *fgfr1/2*$^{UB-/-}$ (21.4 ± 1.8) are reduced compared with control (31.6 ± 0.65) ($P < 0.0001$) and *fgfr1*$^{UB-/-}$ (32.6 ± 1.1) ($P < 0.0001$) (Fig. 5c). Thus, *fgfr2*$^{UB-/-}$ and *fgfr1/2*$^{UB-/-}$ mice have profound defects in ureteric bud development.

We then determined if inappropriate apoptosis and/or a reduction in proliferation contributes to the defects in *fgfr2*$^{UB-/-}$ ureteric bud branching. To assay for apoptosis, we performed fluorescent TUNEL (Terminal Deoxynucleotidyl Transferase-mediated dUTP Nick-End Labeling) assays (Oncogene) on E13.5 (not shown) and E16.5 (Fig. 7) paraffin embryonic sections through regions containing kidneys. On every section examined, at least one or

more *fgfr2*$^{UB-/-}$ ureteric bud tips had clusters of 2–3 apoptotic nuclei (Fig. 7b, arrowhead). In contrast, the vast majority of control ureteric bud tips had no apoptotic nuclei (Fig. 7a); rarely, controls would have one apoptotic nucleus in ureteric tips (not shown). To assay for proliferation, we injected the peritoneum of pregnant E13.5 females with bromodeoxyuridine (BrdU) (Sigma) and then performed immunostaining for BrdU on sections containing kidney. Control ureteric bud tips (Fig. 7c) appeared to have a larger proportion of brown BrdU-positive nuclei than *fgfr2*$^{UB-/-}$ ureteric bud tips (Fig. 7d). Quantitatively, the mean percentage of BrdU uptake in controls (58.7% ± 0.9%) was greater than *fgfr2*$^{UB-/-}$ ureteric bud tips (45.5% ± 1.4%, $P < 0.0001$) (Fig. 7e). Thus, *fgfr2*$^{UB-/-}$ mice have inappropriate regions of apoptosis and decreased rates of proliferation in ureteric bud tips compared with controls.

Fgfr2$^{UB-/-}$ mice develop normal-appearing nephrons, although the numbers are reduced, while fgfr1$^{UB-/-}$ are normal

By hematoxylin and eosin (H&E) staining, *fgfr2*$^{UB-/-}$ embryonic (Fig. 8) and adult kidneys (not shown) have normal-appearing nephrogenic mesenchyme-derived glomeruli (arrowheads) and tubules, as is true in *fgfr1*$^{UB-/-}$ and *fgfr1/2*$^{UB-/-}$ mice (not shown). Immunostaining for Wilm's Tumor Antigen (Wt1) revealed normal glomerular podocyte staining patterns in embryonic kidneys of all genotypes, although the numbers of glomeruli appeared reduced in the *fgfr2*$^{UB-/-}$ and the *fgfr1/2*$^{UB-/-}$ mice (not shown). To quantify glomerular numbers, we grew E11.5 explants for 3 days and then performed whole mount immunostaining for Wt1. As in embryonic kidneys, *fgfr2*$^{UB-/-}$(Fig. 9b) and *fgfr1/2*$^{UB-/-}$ explants (not shown) appeared to have slightly fewer glomeruli compared to control (Fig. 9a) and *fgfr1*$^{UB-/-}$ (not shown). The mean numbers of glomeruli in control (28.6 ± 1.7) and *fgfr1*$^{UB-/-}$ (30.1 ± 1.4) explants were not statistically different, as was the case with *fgfr2*$^{UB-/-}$ (22.3 ± 1.03) and *fgfr1/2*$^{UB-/-}$ explants (20.6 ± 1.4). However, both control and *fgfr1*$^{UB-/-}$ explants had statistically higher mean glomerular numbers than both *fgfr2*$^{UB-/-}$ and *fgfr1/2*$^{UB-/-}$ explants (all $P < 0.0015$) (Fig. 9c). To determine if the reduction in *fgfr2*$^{UB-/-}$ glomerular number persisted into adulthood, we perfused 2-month-old *fgfr2*$^{UB-/-}$ mice and wild type littermates with Alcian blue and counted glomeruli. The *fgfr2*$^{UB-/-}$ adult kidneys had approximately 24% fewer glomeruli than wild type littermates (15948 ± 1186 vs. 21015 ± 1001, respectively) (Fig. 9d); this decrease was strikingly similar to the 22% decrease in *fgfr2*$^{UB-/-}$ explant glomerular number compared with control (Fig. 9c). Thus, although the nephrogenic mesenchyme forms normal structures in mice of all genotypes, absence of *fgfr2* from the ureteric bud does lead to slight decreases in glomerular numbers.

Fgfr2$^{UB-/-}$ mice have patterning abnormalities in cortical stromal mesenchyme

We then determined if there were any defects in cortical stromal patterning in the *fgfr2*$^{UB-/-}$ mice. In situ hybridization with a probe for *Foxd1* revealed aberrantly thickened stroma in subcapsular regions (Fig. 10b, arrow) compared with control kidneys (Fig. 10a, arrow) in E13.5 kidneys. In addition, intercalated stripes of stromal cells seen in control kidneys (Fig. 10, arrowhead) were virtually absent in *fgfr2*$^{UB-/-}$ kidneys (Fig. 10b). Fluorescent TUNEL assays in E13.5 and E16.5 (not shown) kidneys revealed additional abnormalities in mutant stroma with regions of massive subcapsular apoptosis in *fgfr2*$^{UB-/-}$ kidneys (Fig. 10d, concave arrowheads) compared with the relatively minor cortical apoptosis seen in controls

(Fig. 10c, arrowhead). Since similar stromal (and ureteric bud) patterning defects are present in mice with deletion of the *Ret9* isoform (de Graaff et al., 2001) and in mice with interruptions in retinoic acid signaling (which causes *Ret* downregulation) (Batourina et al., 2001; Mendelsohn et al., 1999), we performed in situ hybridization for *Ret*. As in the case of controls (Fig. 10e), $fgfr2^{UB-/-}$ embryonic kidneys do express *Ret* in the peripheral ureteric bud tips in E13.5 kidneys (Fig. 10f, concave arrow). Thus, the $fgfr2^{UB-/-}$ kidneys have patterning defects in cortical stroma as well as in ureteric bud branching, although *Ret* expression is normal.

Discussion

$Fgfr2^{UB-/-}$ mice have profound defects in the ureteric bud lineage, including aberrant branching, thin stalks, fewer total tips, and fewer tips per surface area. These abnormalities are secondary, at least in part, to a reduction in proliferation and inappropriate regions of apoptosis in ureteric bud tips. The nephrogenic mesenchymal lineage in the $fgfr2^{UB-/-}$ mice is much less affected with normal-appearing glomeruli and tubules, and only slightly fewer nephrons than controls. $Fgfr2^{UB-/-}$ kidneys also have thickened stromal mesenchyme with abnormally high rates of apoptosis. The $fgfr1^{UB-/-}$ mice have no apparent renal abnormalities, and there is no additive effect in the $fgfr1/2^{UB-/-}$ kidneys versus the $fgfr2^{UB-/-}$ kidneys. Ultimately, $fgfr2^{UB-/-}$ adult kidneys are small and abnormally shaped or are hydronephrotic.

Despite the abnormalities in the kidneys, the $fgfr2^{UB-/-}$ and $fgfr1/2^{UB-/-}$ post-natal mice appear healthy with apparently normal Mendelian numbers in comparison with the double heterozygous and $fgfr1^{UB-/-}$ mice. One possible explanation is that there are enough residual functioning nephrons in the receptor 2 mutants to avoid renal failure. In support of this hypothesis, on average, both the embryonic explant and adult $fgfr2^{UB-/-}$ mouse kidneys have only approximately a 24% decrease in glomerular number compared with controls. It is also possible that the $fgfr2^{UB-/-}$ and $fgfr1/2^{UB-/-}$ mice have not been aged long enough to detect emerging renal failure in older mice. Finally, perhaps a small subset of $fgfr2^{UB-/-}$ and $fgfr1/2^{UB-/-}$ mice do die shortly after birth, but we have not collected a large enough number of post-natal mice to observe a deviation from the expected Mendelian numbers among the four genotypes.

Unlike the $fgfr2^{UB-/-}$, the $fgfr^{UB-/-}$ mouse kidneys appear normal. One possible explanation is that *fgfr1* is not expressed in the murine ureteric bud. Although a report in the rat does describe *fgfr1* mRNA and protein in the ureteric bud (Cancilla et al., 1999), other published data finds that in the mouse kidney, *fgfr1* expression is confined to glomeruli and other mesenchyme-derived tissues (Peters et al., 1992). Our profiling data by both in situ hybridization and immunofluorescence supports that at least in the mouse, that *fgfr1* is not expressed in the ureteric bud. Although another potential explanation for the normal $fgfr1^{UB-/-}$ phenotype would be that *fgfr1* is incompletely deleted in the ureteric bud, the floxed *fgfr1* mouse has been shown to delete well with other cre lines (Hebert et al., 2003) and our Hoxb7cre mouse efficiently deleted *fgfr2* from the ureteric bud in the $fgfr2^{UB-/-}$ mouse (see Fig. 3e and f). Finally, a third possibility is that FGFR1 is expressed in the mouse ureteric bud (below the sensitivity of our detection assays) but that deletion of the

receptor from the ureteric bud does not result in an obvious renal developmental abnormality.

Although *fgfr2*$^{UB-/-}$ mice have many similar renal defects as in mice with deletions of the *fgfr2-IIIb* receptor isoform or of *fgf* ligands with high degrees of specificity for FGFR2-IIIb (Ohuchi et al., 2000; Qiao et al., 1999; Revest et al., 2001), we detected abnormalities in the *fgfr2*$^{UB-/-}$ mice not described in any of the latter knockout mice. For example, although both *fgfr2*$^{UB-/-}$ mice and *fgf7* knockout mice have small kidneys with fewer ureteric bud branches and slightly fewer nephrons (Qiao et al., 1999), the very aberrant ureteric bud branching, stromal patterning defects, and hydronephrosis seen in adult kidneys was only observed in the *fgfr2*$^{UB-/-}$ mice. Although mice with targeted deletions of *fgfr2-IIIb* and *fgf10* also have small kidneys, the very abnormal ureteric bud branching and stromal patterning defects we describe in the *fgfr2*$^{UB-/-}$ mice were also not reported in the former mice (Ohuchi et al., 2000; Revest et al., 2001) (although hydronephrosis was also not reported in the former mice, both *fgfr2-IIIb* and *fgf10* knockout mice die shortly after birth due to dysplastic lungs, so that abnormalities in adult kidneys cannot be assessed). One possibility is that FGFR2-IIIb is the active FGFR2 isoform in the ureteric bud and that the additional renal developmental abnormalities were simply overlooked in the other mutants. In support of this hypothesis, IIIb isoforms of fibroblast growth factor receptors are generally expressed in epithelial tissues, while IIIc isoforms are found in mesenchymal tissues (Powers et al., 2000). In addition, targeted deletion of *fgfr2-IIIc* results in viable mice with bone and limb anomalies, but no obvious defects in kidney development (Eswarakumar et al., 2002). Another possibility is that differences in background strains and therefore modifier genes result in different phenotypic abnormalities in the *fgfr2*$^{UB-/-}$ conditional knockouts compared with the *fgfr2-IIIb* and the ligand knockouts. A less likely possibility is that due to redundancy of the FGFR2-IIIb and IIIc isoforms, deletion of either alone results in a less severe (or absent) phenotype in the kidney than when both isoforms are removed, as would be the case in the *fgfr2*$^{UB-/-}$ kidneys.

The mechanism by which FGFR2 signaling in the ureteric bud affects both ureteric bud and stromal patterning is unknown. Interestingly, the renal phenotypes we detected in the *fgfr2*$^{UB-/-}$ mice are strikingly similar to abnormalities in mice with targeted deletions of the *Ret9* isoform (de Graaff et al., 2001) or with perturbations of retinoic acid receptor signaling from either vitamin A (precursor to retinoic acid) deprivation (Batourina et al., 2001) or deletion of both retinoic acid receptors (RAR) a and b2 (Mendelsohn et al., 1999). Moreover, interruption of retinoic acid signaling results in downregulation of *Ret* expression on the ureteric bud, while forced expression of *Ret* in *Rara/Rarb2*$^{-/-}$ double knockout mice completely rescues the ureteric bud and stromal patterning defects (Batourina et al., 2001). Despite the similar renal developmental anomalies between the *fgfr2*$^{UB-/-}$ mice and the other mutant mice, the presence of *Ret* in *fgfr2*$^{UB-/-}$ kidneys strongly suggests that FGFR2 signaling is not upstream of the retinoic acid/Ret signaling loop. Whether FGFR2 activity or expression is dependent on retinoic acid or Ret signaling is unknown. Another interesting possibility, however, is that Ret and FGFR2, both receptor tyrosine kinases that are expressed in the ureteric bud and that share at least one major signaling adapter molecule

(Hadari et al., 2001; Melillo et al., 2001), may have common downstream target(s) that mediate ureteric bud and/or stromal patterning.

Acknowledgments

We thank Dr. Fenglei Jiang for her contributions to the study and Cindy McAllister for her assistance with the confocal microscopy. We also thank Reena Shakya and Dr. Frank Costantini for the Hoxb7 promoter construct, Dr. Janet Rossant for the floxed *fgfr1* mice, Dr. David Ornitz for the floxed *fgfr2* mice, and Dr. Larry Patterson for the *Foxd1* probe template. This study was supported by grants from the National Institute of Child Health and Human Development, 5 P30 HD34615-02 (C. M. B.), and the National Institute of Diabetes and Digestive and Kidney Disease, DK-41612 (M. B.).

References

Arman E, Haffner-Krausz R, Chen Y, Heath JK, Lonai P. Targeted disruption of fibroblast growth factor (FGF) receptor 2 suggests a role for FGF signaling in pregastrulation mammalian development. Proc Natl Acad Sci U S A. 1998; 95:5082–5087. [PubMed: 9560232]

Bankir L, Hollenberg NK. In vivo staining of the kidney with Alcian blue: an adjunct to morphological and physiological studies. Ren Physiol. 1983; 6:151–155. [PubMed: 6191372]

Bates CM, Merenmies JM, Kelly-Spratt KS, Parada LF. Insulin receptor-related receptor expression in non-A intercalated cells in the kidney. Kidney Int. 1997; 52:674–681. [PubMed: 9291186]

Bates CM, Kharzai S, Erwin T, Rossant J, Parada LF. Role of N-myc in the developing mouse kidney. Dev Biol. 2000; 222:317–325. [PubMed: 10837121]

Bates CM, Kegg H, Petrevski C, Grady S. Expression of somatostatin receptors 3, 4, and 5 in mouse kidney proximal tubules. Kidney Int. 2003; 63:53–63. [PubMed: 12472768]

Batourina E, Gim S, Bello N, Shy M, Clagett-Dame M, Srinivas S, Costantini F, Mendelsohn C. Vitamin A controls epithelial/mesenchymal interactions through Ret expression. Nat Genet. 2001; 27:74–78. [PubMed: 11138002]

Cancilla B, Ford-Perriss MD, Bertram JF. Expression and localization of fibroblast growth factors and fibroblast growth factor receptors in the developing rat kidney. Kidney Int. 1999; 56:2025–2039. [PubMed: 10594778]

Celli G, LaRochelle WJ, Mackem S, Sharp R, Merlino G. Soluble dominant-negative receptor uncovers essential roles for fibroblast growth factors in multi-organ induction and patterning. EMBO J. 1998; 17:1642–1655. [PubMed: 9501086]

Colvin JS, Bohne BA, Harding GW, McEwen DG, Ornitz DM. Skeletal overgrowth and deafness in mice lacking fibroblast growth factor receptor 3. Nat Genet. 1996; 12:390–397. [PubMed: 8630492]

Damadian RV, Shwayri E, Bricker NS. On the existence of non-urine forming nephrons in the diseased kidney of the dog. J Lab Clin Med. 1965; 65:26–39. [PubMed: 14260693]

de Graaff E, Srinivas S, Kilkenny C, D'Agati V, Mankoo BS, Costantini F, Pachnis V. Differential activities of the RET tyrosine kinase receptor isoforms during mammalian embryogenesis. Genes Dev. 2001; 15:2433–2444. [PubMed: 11562352]

Deng CX, Wynshaw-Boris A, Shen MM, Daugherty C, Ornitz DM, Leder P. Murine FGFR-1 is required for early postimplantation growth and axial organization. Genes Dev. 1994; 8:3045–3057. [PubMed: 8001823]

Dudley AT, Godin RE, Robertson EJ. Interaction between FGF and BMP signaling pathways regulates development of metanephric mesenchyme. Genes Dev. 1999; 13:1601–1613. [PubMed: 10385628]

Eswarakumar VP, Monsonego-Ornan E, Pines M, Antonopoulou I, Morriss-Kay GM, Lonai P. The IIIc alternative of Fgfr2 is a positive regulator of bone formation. Development. 2002; 129:3783–3793. [PubMed: 12135917]

Fuhrmann V, Kinkl N, Leveillard T, Sahel J, Hicks D. Fibroblast growth factor receptor 4 (FGFR4) is expressed in adult rat and human retinal photoreceptors and neurons. J Mol Neurosci. 1999; 13:187–197. [PubMed: 10691305]

Gilbert T, Lelievre-Pegorier M, Malienou R, Meulemans A, Merlet-Benichou C. Effects of prenatal and postnatal exposure to gentamicin on renal differentiation in the rat. Toxicology. 1987; 43:301–313. [PubMed: 3824397]

Hadari YR, Gotoh N, Kouhara H, Lax I, Schlessinger J. Critical role for the docking-protein FRS2 alpha in FGF receptor-mediated signal transduction pathways. Proc Natl Acad Sci U S A. 2001; 98:8578–8583. [PubMed: 11447289]

Hebert JM, Lin M, Partanen J, Rossant J, McConnell SK. FGF signaling through FGFR1 is required for olfactory bulb morphogenesis. Development. 2003; 130:1101–1111. [PubMed: 12571102]

Klint P, Claesson-Welsh L. Signal transduction by fibroblast growth factor receptors. Front Biosci. 1999; 4:D165–D177. [PubMed: 9989949]

Kuure S, Vuolteenaho R, Vainio S. Kidney morphogenesis: cellular and molecular regulation. Mech Dev. 2000; 92:31–45. [PubMed: 10704886]

Melillo RM, Santoro M, Ong SH, Billaud M, Fusco A, Hadari YR, Schlessinger J, Lax I. Docking protein FRS2 links the protein tyrosine kinase RET and its oncogenic forms with the mitogen-activated protein kinase signaling cascade. Mol Cell Biol. 2001; 21:4177–4187. [PubMed: 11390647]

Mendelsohn C, Batourina E, Fung S, Gilbert T, Dodd J. Stromal cells mediate retinoid-dependent functions essential for renal development. Development. 1999; 126:1139–1148. [PubMed: 10021334]

Ohuchi H, Hori Y, Yamasaki M, Harada H, Sekine K, Kato S, Itoh N. FGF10 acts as a major ligand for FGF receptor 2 IIIb in mouse multi-organ development. Biochem Biophys Res Commun. 2000; 277:643–649. [PubMed: 11062007]

Ortiz LA, Quan A, Weinberg A, Baum M. Effect of prenatal dexamethasone on rat renal development. Kidney Int. 2001; 59:1663–1669. [PubMed: 11318936]

Ortiz LA, Quan A, Zarzar F, Weinberg A, Baum M. Prenatal dexamethasone programs hypertension and renal injury in the rat. Hypertension. 2003; 41:328–334. [PubMed: 12574103]

Peters KG, Werner S, Chen G, Williams LT. Two FGF receptor genes are differentially expressed in epithelial and mesenchymal tissues during limb formation and organogenesis in the mouse. Development. 1992; 114:233–243. [PubMed: 1315677]

Powers CJ, McLeskey SW, Wellstein A. Fibroblast growth factors, their receptors and signaling. Endocr-Relat Cancer. 2000; 7:165–197. [PubMed: 11021964]

Qiao J, Uzzo R, Obara-Ishihara T, Degenstein L, Fuchs E, Herzlinger D. FGF-7 modulates ureteric bud growth and nephron number in the developing kidney. Development. 1999; 126:547–554. [PubMed: 9876183]

Revest JM, Spencer-Dene B, Kerr K, De Moerlooze L, Rosewell I, Dickson C. Fibroblast growth factor receptor 2-IIIb acts upstream of Shh and Fgf4 and is required for limb bud maintenance but not for the induction of Fgf8 Fgf10, Msx1, or Bmp4. Dev Biol. 2001; 231:47–62. [PubMed: 11180951]

Soriano P. Generalized lacZ expression with the ROSA26 Cre reporter strain. Nat Genet. 1999; 21:70–71. [PubMed: 9916792]

Srinivas S, Goldberg M, Watanabe T, D'Agati V, Costantini F. Expression of green fluorescent protein in the ureteric bud of transgenic mice: a new tool for the analysis of ureteric bud morphogenesis. Dev Genet. 1999a; 24:241–251. [PubMed: 10322632]

Srinivas S, Wu Z, Chen C, D'Agati V, Costantini F. Dominant effects of RET receptor misexpression and ligand-independent RET signaling on ureteric bud development. Development. 1999b; 126:1375–1386. [PubMed: 10068631]

Weinstein M, Xu X, Ohyama K, Deng CX. FGFR-3 and FGFR-4 function cooperatively to direct alveogenesis in the murine lung. Development. 1998; 125:3615–3623. [PubMed: 9716527]

Xu X, Weinstein M, Li C, Naski M, Cohen RI, Ornitz DM, Leder P, Deng C. Fibroblast growth factor receptor 2 (FGFR2)-mediated reciprocal regulation loop between FGF8 and FGF10 is essential for limb induction. Development. 1998; 125:753–765. [PubMed: 9435295]

Yamaguchi TP, Harpal K, Henkemeyer M, Rossant J. fgfr-1 is required for embryonic growth and mesodermal patterning during mouse gastrulation. Genes Dev. 1994; 8:3032–3044. [PubMed: 8001822]

Yu J, Carroll TJ, McMahon AP. Sonic hedgehog regulates proliferation and differentiation of mesenchymal cells in the mouse metanephric kidney. Development. 2002; 129:5301–5312. [PubMed: 12399320]

Yu K, Xu J, Liu Z, Sosic D, Shao J, Olson EN, Towler DA, Ornitz DM. Conditional inactivation of FGF receptor 2 reveals an essential role for FGF signaling in the regulation of osteoblast function and bone growth. Development. 2003; 130:3063–3074. [PubMed: 12756187]

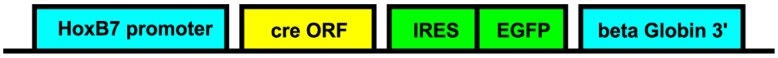

Fig. 1.

Hoxb7creEGFP transgenic construct. Hoxb7 promoter (blue), cre recombinase open reading frame (yellow), internal ribosomal entry site, enhanced green fluorescent protein (green), and human β globin poly-A tail (blue).

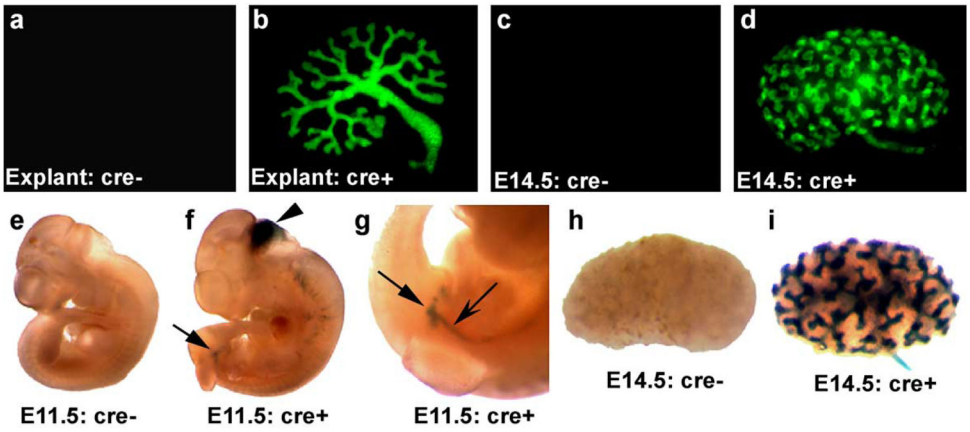

Fig. 2.

GFP and cre expression patterns in the Hoxb7creEGFP transgenic mouse. (a–d) GFP is expressed in ureteric bud tissues in Hoxb7creEGFP-positive E11.5 kidney explants (b) and E14.5 kidneys (d) but not in cre-negative littermate explants (a) or E14.5 kidneys (c). (e–g) In E11.5 embryos, G*trosa*-positive/Hoxb7creEGFP mice (f, g) show X-gal staining in the ureteric bud (arrows), Wolffian duct (concave arrow), hindbrain (arrowhead), while G*trosa*-positive/cre-negative littermates (e) show no signal. (h, i) Similarly, at E14.5 G*trosa*-positive/cre-positive kidneys show X-gal staining throughout the ureteric bud tree (i), while G*trosa*-positive/cre-negative littermate kidneys (h) show no signal. (a, b = 40× magnifications; c, d, g–i = 25× magnifications; e, f = 10± magnifications).

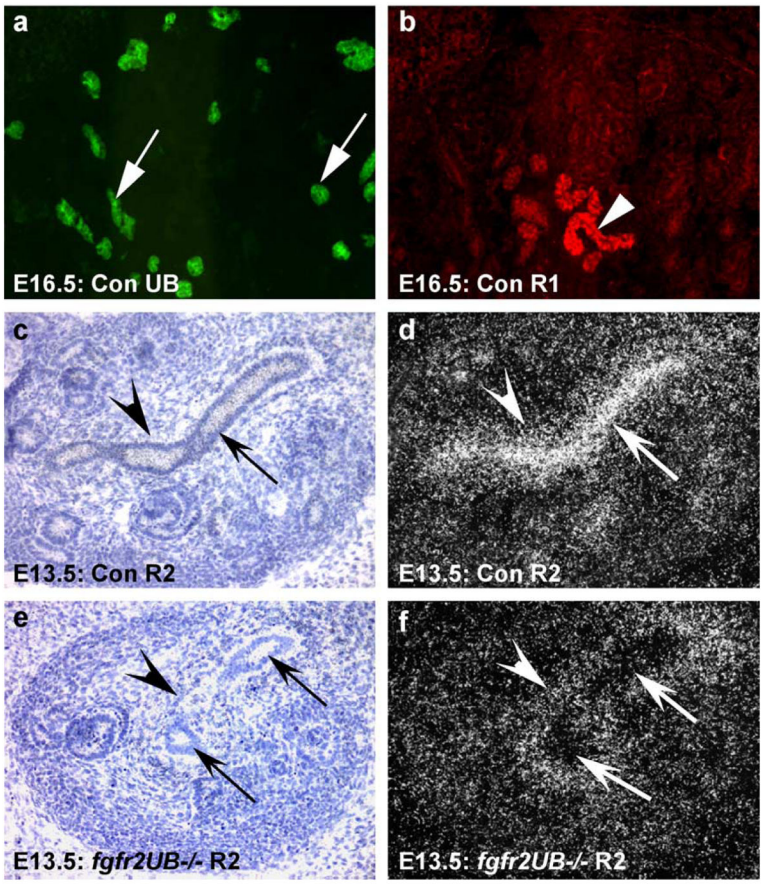

Fig. 3.

Fibroblast growth factor receptor 1 and 2 staining patterns in embryonic kidneys. (a, b) In a control Hoxb7creEGFP-positive E16.5 kidney, immunostaining in adjacent sections reveals that FGFR1-expressing tubules (b, arrowhead) are not GFP-positive ureteric bud epithelia (a, arrows). (c, d) In a control E13.5 kidney section, brightfield (c) and darkfield (d) images show intense *fgfr2* signal by in situ hybridization in ureteric bud epithelia (concave arrows) and moderate signal in mesenchyme-derived tissues especially those surrounding the ureteric bud (concave arrowheads). (e, f) In an $fgfr2^{UB-/-}$ E13.5 kidney section, brightfield (e) and darkfield (f) images demonstrate absence of *fgfr2* signal in the ureteric bud by in situ hybridization (concave arrows), but persistence of mesenchyme-derived signal including tissues surrounding the ureteric bud (concave arrowheads). (All = 200× magnifications).

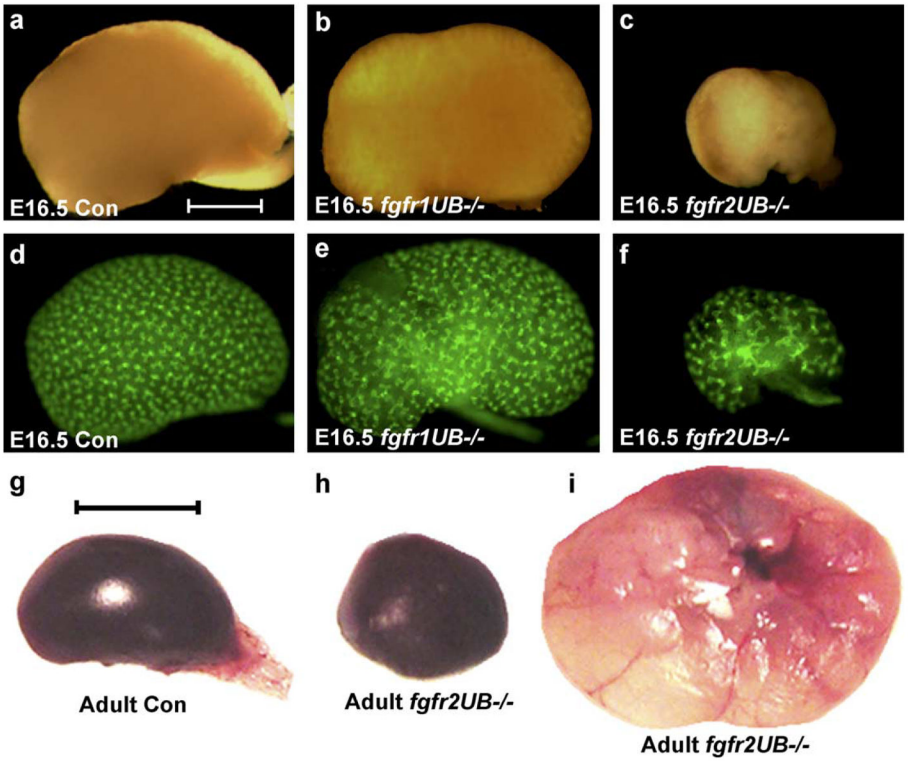

Fig. 4.

Gross comparison between control, *fgfr1*$^{UB-/-}$ and *fgfr2*$^{UB-/-}$ kidneys. (a–c) Comparison of E16.5 control double heterozygous (a), *fgfr1*$^{UB-/-}$ (b) and *fgfr2*$^{UB-/-}$ kidneys under direct light (c). (d–f) Comparison of the same E16.5 kidneys under fluorescent light revealing GFP-positive ureteric bud tissues. (g–i) Adult (6 week) kidneys from a control mouse (g) and a littermate *fgfr2*$^{UB-/-}$ mouse with a small, abnormally shaped kidney (h) and a hydronephrotic kidney (i). White scale bar = 0.5 mm. Black scale bar = 0.5 cm.

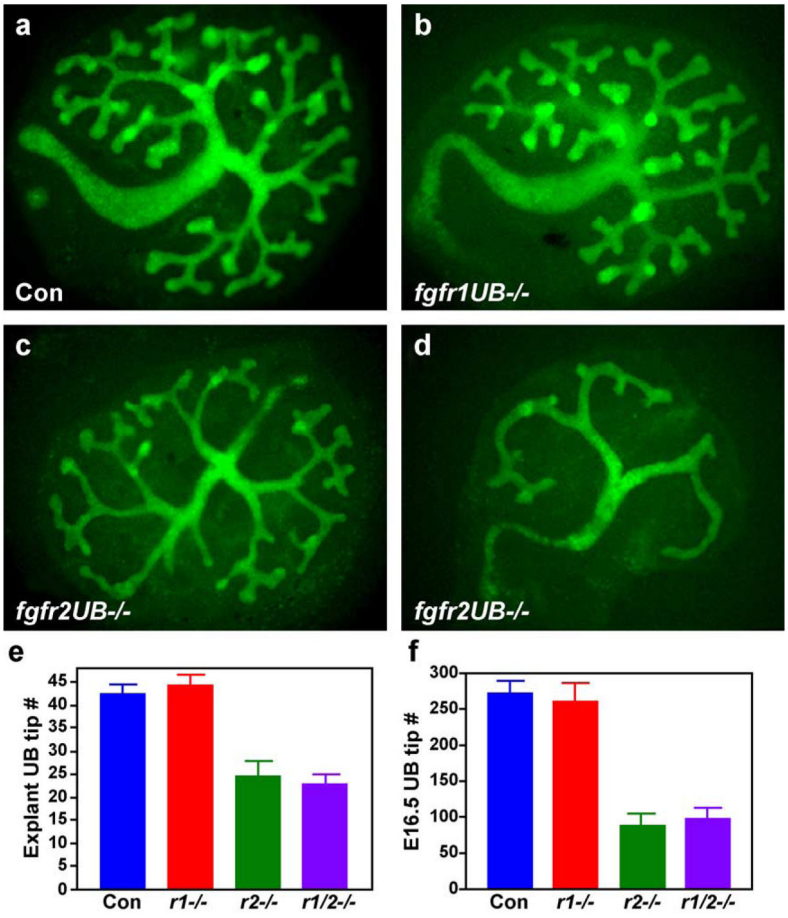

Fig. 5.

Comparison of ureteric bud branching and ureteric bud tip numbers in control, *fgfr1*$^{UB-/-}$, *fgfr2*$^{UB-/-}$, and *fgfr*1/2$^{UB-/-}$ embryonic kidneys. (a–d) Fluorescent micrographs of E11.5 explants demonstrating that control (a) and *fgfr1*$^{UB-/-}$(b) are indistinguishable, while *fgfr2*$^{UB-/-}$ explants (c, d) have thin, long ureteric trunks and fewer ureteric bud tips, with a range of phenotype severity (a–d = 40× magnifications). (e) Bar graph of E11.5 explant ureteric bud tip numbers, showing that control ($N = 16$) and *fgfr1*$^{UB-/-}$ ($N = 14$) are both different than *fgfr2*$^{UB-/-}$ ($N = 8$) ($P < 0.0001$) and *fgfr1/2*$^{UB-/-}$ ($N = 8$) ($P < 0.0001$). (f) Bar graph of E16.5 kidney ureteric bud tip counts from confocal images, demonstrating that control ($N = 18$) and *fgfr1*$^{UB-/-}$ ($N = 8$) are both different than *fgfr2*$^{UB-/-}$ ($N = 12$) ($P < 0.0001$) and *fgfr1/2*$^{UB-/-}$ ($N = 14$). ($P < 0.0001$).

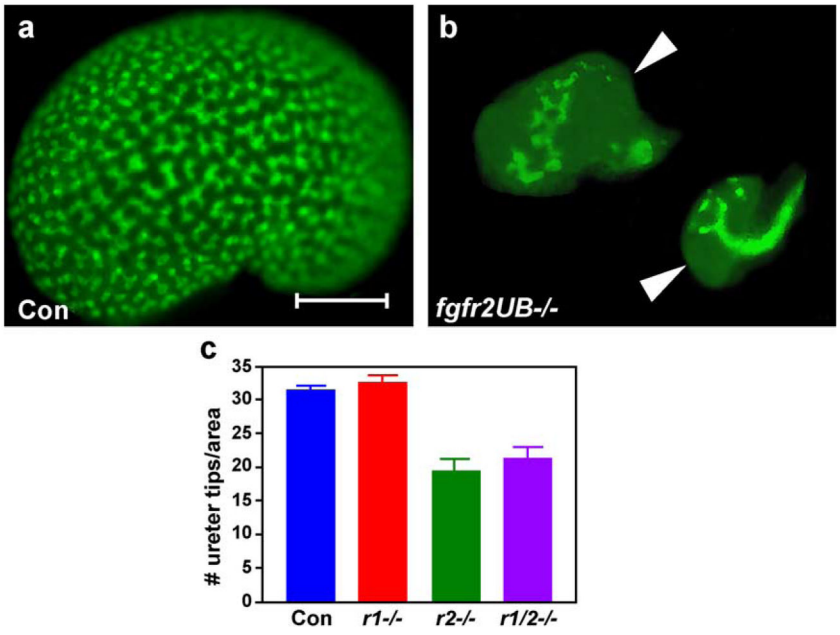

Fig. 6.

Comparison of ureteric bud tip numbers/surface area in control, *fgfr1*$^{UB-/-}$, *fgfr2*$^{UB-/-}$, and *fgfr1/2*$^{UB-/-}$ E16.5 kidneys. (a–b) Fluorescent micrographs of E16.5 littermate kidneys showing that compared to controls (a), many *fgfr2*$^{UB-/-}$ kidneys (b) have large areas devoid of ureteric bud tissues (arrowheads). (Scale bar = 0.5 mm). (c) Bar graph of E16.5 kidney ureteric bud tip numbers/surface area from confocal images showing that control (N = 18) and *fgfr1*$^{UB-/-}$ (N = 8) are both different than *fgfr2*$^{UB-/-}$ (N = 12) (P < 0.0001) and *fgfr1/2*$^{UB-/-}$ (N = 14) (P < 0.0001).

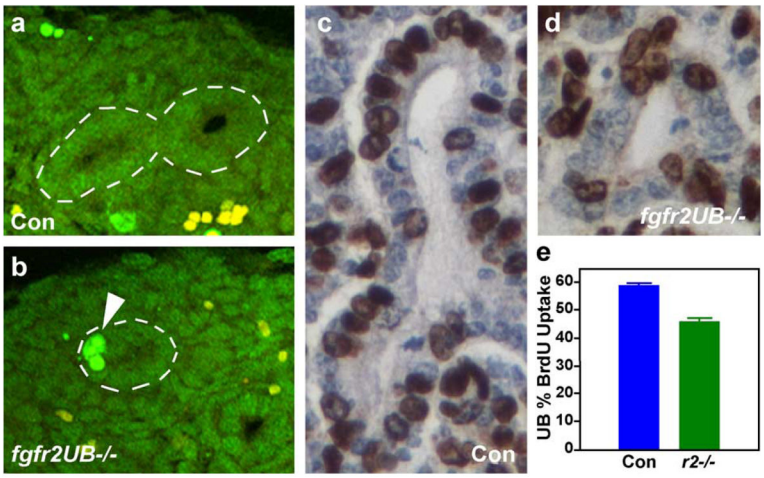

Fig. 7.

Comparison of apoptosis pattern and proliferation rates in control and *fgfr2*$^{UB-/-}$ ureteric bud tips (dotted lines). (a–b) Fluorescent TUNEL assays in E16.5 kidneys demonstrating no apoptosis in control ureteric bud tips (a) and 3 apoptotic green nuclei in an *fgfr2*$^{UB-/-}$ ureteric bud tip (b, arrowhead). (Yellow staining is non-specific). (c–d) Light micrographs in E13.5 kidneys showing more apparent BrdU labeling in control ureteric bud tip nuclei (c) than in *fgfr2*$^{UB-/-}$ ureteric bud tip nuclei (d). (a–d = 400× magnifications). (e) Bar graph demonstrating that E13.5 control ureteric bud tips ($N = 6$) have a higher percentage of BrdU uptake than *fgfr2*$^{UB-/-}$ ($N = 6$) ($P < 0.0001$).

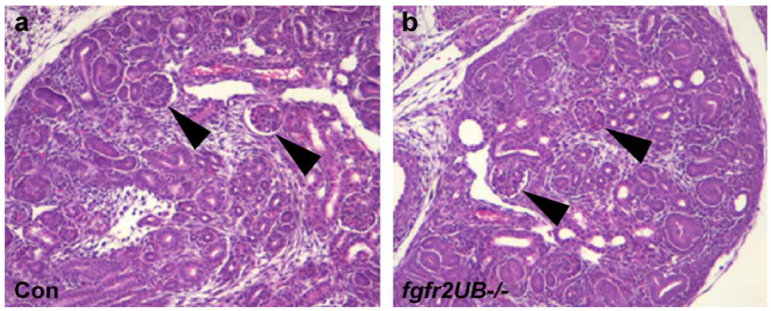

Fig. 8.

Comparison of control and *fgfr2*$^{UB-/-}$ developing nephrons by H and E staining. Light micrographs showing that E16.5 control (a) and *fgfr2*$^{UB-/-}$ (b) kidneys both have normal appearing glomeruli (arrowheads) and no tubular dysplasia (both = 40× magnifications).

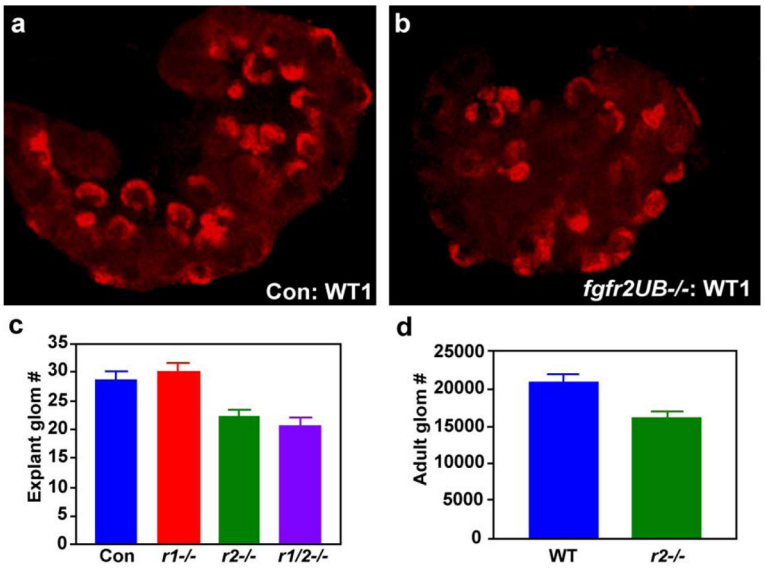

Fig. 9.

Comparison of glomerular numbers in control, *fgfr1*$^{UB-/-}$, *fgfr2*$^{UB-/-}$, and *fgfr1/2*$^{UB-/-}$ kidneys. (a, b) Whole mount Wt1 immunofluorescence in E11.5 explants demonstrating that controls (a) have more glomeruli than *fgfr2*$^{UB-/-}$ (b). (a, b = 40× magnifications). (c) Bar graph of explant glomerular numbers showing that control ($N = 8$) and *fgfr1*$^{UB-/-}$ ($N = 7$) are both different than *fgfr1/2*$^{UB-/-}$ ($N = 8$) ($P < 0.0005$) and *fgfr2*$^{UB-/-}$ ($N = 14$) (control vs. *fgfr2*$^{UB-/-}$ $P = 0.0012$; *fgfr1*$^{UB-/-}$ vs. *fgfr2*$^{UB-/-}$ $P < 0.0005$). (d) Bar graph demonstrating that in adult mice, wild type kidneys ($N = 14$) have more glomeruli *fgfr2*$^{UB-/-}$ kidneys ($N = 12$) ($P = 0.0031$).

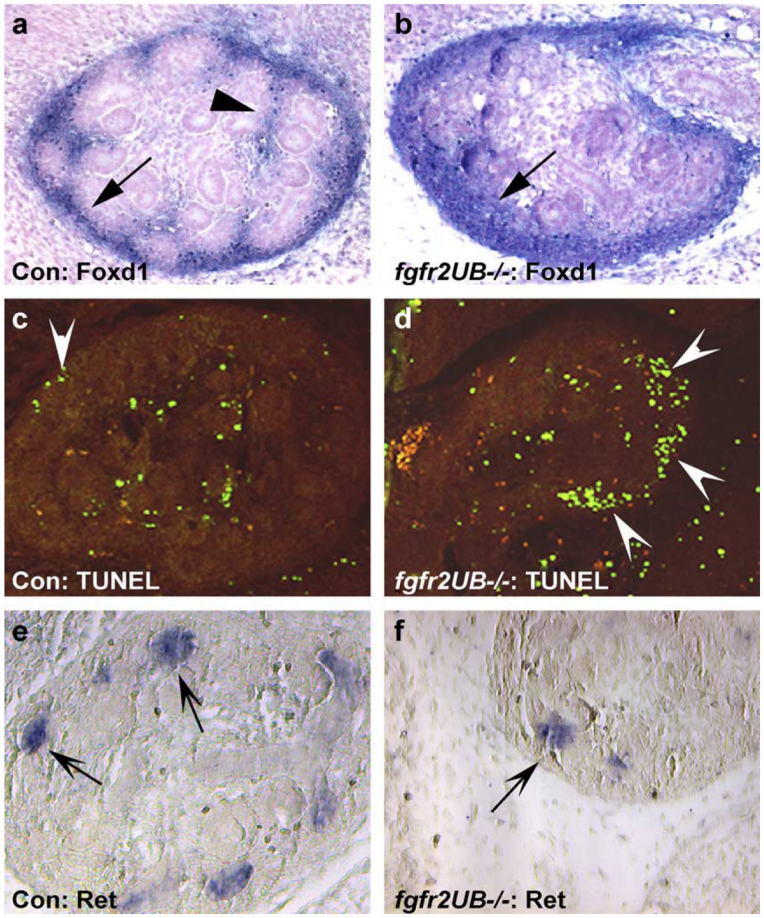

Fig. 10.

Comparison of cortical stromal patterning and Ret expression in control and *fgfr2*$^{UB-/-}$ E13.5 kidneys. (a, b) *Foxd1* in situ hybridization demonstrating that controls have normal subcapsular cortical stromal thickness (a, arrow) and intercalated stripes of stroma (a, arrowhead) compared with *fgfr2*$^{UB-/-}$ kidneys that have aberrantly thickened subcapsular stroma (b, arrow) and absence of intercalated stripes of stroma (b). (c, d) Fluorescent TUNEL images showing minimal apoptosis in cortical stroma of control kidneys (c, concave arrowhead), but regions of extensive apoptosis in subcapsular cortical stroma in *fgfr2*$^{UB-/-}$ kidneys (d, concave arrowhead). (e, f) In situ hybridization demonstrating normal *Ret* expression in control and *fgfr2*$^{UB-/-}$ ureteric bud tips. (All = 200× magnifications).

Table 1

PCR primer constructs

Gene	Primer pairs	Size (BP)
Hoxb7cre EGFP	5′-AGCGCGATCACA TGGTCCTG-3′	230
	5′-ACGATCCTGAGACTTCCACACT-3′	
fgfr1	5′-TTGACCGGATCTACACACACC-3′	602 (wt)
	5′-AAGCCACCATCACCTGAGGAA-3′	672 (floxed)
fgfr2	5′-GTCAATTCTAAGCCACTGTCTGCC-3′	307 (wt)
	5′-CTCCACTGATTACATCTAAAGAGC-3′	373 (floxed)

Table 2

Possible outcomes in progeny from (Hoxb7creEGFP$^{+/-}$, *fgfr1*$^{lox/+}$, *fgfr2*$^{lox/+}$) × (*fgfr1*$^{lox/lox}$, *fgfr2*$^{lox/lox}$)

	***fgfr1*$^{lox/lox}$, *fgfr2*$^{lox/+}$**	***fgfr1*$^{lox/+}$, *fgfr2*$^{lox/lox}$**	***fgfr1*$^{lox/lox}$, *fgfr2*$^{lox/lox}$**	***fgfr1*$^{lox/+}$, *fgfr2*$^{lox/+}$**
Hoxcre$^{+/-}$	UB deletion of *fgfr1* (*fgfr1*$^{UB-/-}$)	UB deletion of *fgfr2* (*fgfr2*$^{UB-/-}$)	UB deletion of *fgfr1* and *2* (*fgfr1/2*$^{UB-/-}$)	double heterozygotes
Hoxcre$^{-/-}$	no deletion	no deletion	no deletion	no deletion

UB = ureteric bud.

Table 3

Distribution of genotypes among the adult live-born hoxb7cre+ mice (from breeding scheme outlined in Table 2)

Genotype	Double heterozygous	*fgfr1*$^{UB-/-}$	*fgfr2*$^{UB-/-}$	*fgfr1/2*$^{UB-/-}$
# mice	10	7	9	10